J Solid State Electrochem (2008) 12:1399–1404
DOI 10.1007/s10008-007-0476-0

ORIGINAL PAPER

On the charge storage mechanism at RuO_2/0.5 M H_2SO_4 interface

K. Juodkazis · J. Juodkazytė · V. Šukienė · A. Grigucevičienė · A. Selskis

Received: 11 September 2007 / Revised: 19 October 2007 / Accepted: 20 October 2007 / Published online: 4 December 2007

Abstract Comparative study of capacitative properties of RuO_2/0.5 M H_2SO_4 and Ru/0.5 M H_2SO_4 interfaces has been performed with a view to find out the nature of electrochemical processes involved in the charge storage mechanism of ruthenium (IV) oxide. The methods of cyclic voltammetry and scanning electron microscopy (SEM) were employed for the investigation of electrochemical behavior and surface morphology of RuO_2 electrodes. It has been suggested that supercapacitor behavior of RuO_2 phase in the potential E range between 0.4 and 1.4 V vs reference hydrogen electrode (RHE) should be attributed to double-layer-type capacitance, related to non-faradaic highly reversible process of $RuO_2^+ \cdot (OH^-)_{ad}$ ionic pair formation and annihilation at RuO_2/electrolyte interface as described by following summary equation:

$$RuO_2 \cdot H_2O \Leftrightarrow RuO_2^+ \cdot (OH^-)_{ad} + H^+ + e^-_{(CB)},$$

where RuO_2^+ and $e^-_{(CB)}$ represent holes and electrons in valence and conduction bands, respectively. The pseudocapacitance of interface under investigation is related to partial reduction of RuO_2 layer at $E<0.2$ V and its subsequent recovery during the anodic process.

Keywords RuO_2 · Electrochemical supercapacitors · Charge storage mechanism

K. Juodkazis (✉) · J. Juodkazytė · V. Šukienė · A. Grigucevičienė · A. Selskis
Institute of Chemistry,
A. Goštauto 9,
LT-01108 Vilnius, Lithuania
e-mail: kesjuod@ktl.mii.lt

Introduction

Hydrous ruthenium dioxide, $RuO_2 \cdot xH_2O$, represents promising material to be employed in electrochemical capacitors or the so-called supercapacitors. It has been reported that specific capacitance C^{sp} of nano/micro-metric layers of RuO_2 coated on the conducting inert substrate with large specific surface, e.g., activated carbon, exceeds thousands of farads per 1 g of RuO_2 [1, 2]. Generally, the overall capacitance of electrochemical capacitors is supposed to consist of double-layer capacitance, C_{DL}, arising from charge separation at the electrode/electrolyte interface, and pseudocapacitance, C_{PC}, determined by faradaic redox processes taking place at the electrode surface. In the case of $RuO_2 \cdot xH_2O$, pseudocapacitance is considered to play predominant role in charging process [3–5], and the charge storage mechanism is described by the following equation:

$$RuO_x(OH)_y + \delta H^+ + \delta e^- \Leftrightarrow RuO_{x-\delta}(OH)_{y+\delta} \quad (1)$$

proposed by Trasatti and Buzzanca [6]. It is believed that highly reversible redox transitions between Ru(II)/Ru(III), Ru(III)/Ru(IV) [3], and Ru(IV)/Ru(VI) [2] taking place within $RuO_2 \cdot xH_2O$ phase are involved in pseudocapacitative charging and discharging mechanism. According to Eq. 1, $RuO_2 \cdot xH_2O$ should behave like mixed electron/proton conductor, and effective electron and proton transport pathways are necessary for the efficient charge storage. The former ones are predetermined by electronic conductivity of $RuO_2 \cdot xH_2O$ [7], whereas the latter ones are provided by the presence of structural water. The influence of structural H_2O on the capacitative properties of hydrous ruthenium oxide should be particularly emphasized. Firstly, it is known that anhydrous crystalline RuO_2 is good electronic conductor, but poor capacitor, whereas amorphous hydrous $RuO_2 \cdot xH_2O$ is good capacitor with lower

electronic, yet better ionic conductivity [8]. Moreover, nuclear magnetic resonance (NMR) spectroscopic study [9] has shown that dependence of $RuO_2{\cdot}xH_2O$ specific capacitance on the structural water content, x, goes through a maximum at $x\approx0.85$, i.e., at the point where the nominal composition of the oxide approaches $RuO_2{\cdot}H_2O$. Practically, the same result was obtained independently by Zheng et al. [10] on the basis of electrochemical measurements performed with sol–gel-derived $RuO_2{\cdot}xH_2O$ powders annealed at various temperatures. Naturally, structural water content and, hence, the specific capacitance of $RuO_2{\cdot}xH_2O$ should be strongly dependent on ruthenium oxide synthesis method and electrode pretreatment conditions. Therefore, it is not surprising that C^{sp} values reported in literature for various $RuO_2{\cdot}xH_2O$ samples differ significantly [1, 2, 8, 9, 11].

On the basis of potential scan rate, v dependence of nanoparticulate RuO_2 capacitance, Sugimoto et al. [12, 13] have deconvoluted the overall C into v-independent C_{DL} and pseudocapacitance C_{PC} related to reversible and irreversible faradaic redox processes. In the case of anhydrous RuO_2, it has been found [12] that pseudocapacitance makes ~60% of the overall C at scan rates as low as 0.5 mV s^{-1}, whereas at 500 mV s^{-1}, it is just about 10% of the overall C, which means that C_{DL} constitutes the major part of the overall capacitance. In the case of hydrous RuO_2 with nominal composition of $RuO_2{\cdot}H_2O$, the portion of C_{PC} at low scan rate increased up to ~70% [13]. The authors, however, gave no concrete suggestion regarding the nature of the processes involved in double layer and pseudocapacitative charging. It is known that anhydrous RuO_2, which forms on ruthenium electrode at $E>0.8$ V and passivates the surface, is hardly reducible even at $E<0$ V [14]. Thus, it is unclear how the aforementioned highly reversible redox transitions between various Ru oxidation states can occur within the RuO_2 phase.

In the present study, the mechanism of faradaic and non-faradaic charging processes at RuO_2/0.5 M H_2SO_4 interface has been analyzed in the case of electrochemically and thermally formed layers of RuO_2 on Ti and Au substrates with a view to find out the nature of these processes. The electrochemical behavior of metallic ruthenium electrode prepared in form of Ru electroplate has been also studied.

Experimental

The equipment used for voltammetric measurements is described in detail elsewhere [15].

To produce working electrodes, ruthenium coating (~1 μm thick) was deposited electrochemically from acid $RuOHCl_3$ electrolyte either directly on titanium (~99.9%) wire (∅=4 mm) activated chemically in diluted H_2SO_4 (1:1) at 353 K for 2–3 min or on gold-plated titanium substrate. Thickness of gold underlayer was 0.1–0.2 μm.

Electrochemical formation of RuO_2 layer was performed as follows: ~1-μm thick ruthenium coating on Ti substrate was anodized at 1.45 V, i.e., in O_2 evolution region in the solution of 0.5 M H_2SO_4 for 30 min. The formation of brown RuO_2 layer could be seen visibly.

To prepare the RuO_2 electrode thermally, four to six layers of $RuOHCl_3$ solution were painted onto Au substrate, with each layer heated preliminary at 673 K for 10 to 15 min to ensure the adhesion, and then heated additionally for 1 h at 673 K. The amount of RuO_2 deposited on the electrode was about 0.45 mg cm^{-2}, which corresponds to oxide layer thickness of ~0.6 μm.

A conventional three-compartment glass cell was used for the measurements. Pure Pt (99.99%) plate served as a counter electrode. Hydrogen electrode in a working solution (RHE) was used as reference. Current and charge density values in the text refer to apparent surface area of the electrode.

Sulfuric acid of analytical grade and triply distilled water were used to prepare the solutions. All electrochemical measurements were carried out in inert argon atmosphere at room temperature (293 K).

Surface morphology of RuO_2 electrodes was investigated using Scanning Electron Microscope EVO 50 EP (Carl Zeiss SMT AG, Germany).

Results and discussion

Figure 1a displays cyclic voltammograms of RuO_2 layer formed electrochemically on Ru-plated titanium substrate in the solution of 0.5 M H_2SO_4. Cycle 1 in Fig. 1a illustrates the well-known rectangular-shaped voltammetric response, where anodic and cathodic current density i is practically independent of potential E over the range from ~0.6 to ~1.4 V. Figure 2a illustrates the dependence of electrochemically formed RuO_2 electrode capacitance on potential scan rate within 0.4 V$<E<$1.2 V. One can see that within 0.6 V$<E<$1.2 V, C is practically independent of E and v, as the latter changes from 10 to 100 mV s^{-1}. Such behavior is not typical for faradaic electrochemical processes. The electrode in this case behaves like electrochemical double-layer capacitor with almost constant capacitance in accordance with well-know equation:

$$C = i_{cap}/v, \tag{2}$$

where i_{cap} is capacitative current and v is potential scan rate. Extension of potential cycling range in cycles 2 and 3 of Fig. 1a reveals the beginning of oxygen evolution at $E>$ 1.4 V and also the beginning of RuO_2 layer reduction/destruction process at $E<0.4$ V. This process gains momentum at more cathodic potentials, i.e., at $E<0.2$ V, as evident from the negative going scan of cycle 3 (Fig. 1a).

The products of cathodic reduction are oxidized in subsequent anodic scan, as revealed by anodic current wave spanning the whole E range up to oxygen evolution reaction. It is noteworthy that after such treatment, the shape of the cathodic part of the voltammogram remains essentially the same, indicating that RuO_2 layer has been completely recovered.

Very similar results, in terms of voltammetric and capacitative behavior, were obtained in the case of thermally formed RuO_2 layer on Au substrate (Figs. 1b and 2b). Heated at 673 K, RuO_2 is considered to be anhydrous [10], although certain rehydration of the RuO_2 layer surface in 0.5 M H_2SO_4 cannot be excluded, as demonstrated recently in the EQCM study [16]. One can see that voltammograms in Fig. 1b reveal better-pronounced, compared to Fig. 1a, anodic and cathodic current waves at 0.4–0.9 and 0.9–1.2 V, which can be related to the aforementioned faradaic redox processes between Ru(III)/Ru(IV) or Ru(IV)/Ru(VI), respectively. This can also be seen in Fig. 2b, where the dependence of capacitance on potential scan rate is also more vivid than in Fig. 2a, pointing to a larger contribution of pseudocapacitance, although the amount of charge corresponding to these faradaic processes and, consequently to C_{PC}, is insignificant. Such behavior may be due to the presence of small amounts of metallic ruthenium in RuO_2 phase, which can form in the course of thermal decomposition of $RuOHCl_3$ as demonstrated recently in Santos et al. [17]. The specific capacitance, C^{sp}, of thermally formed RuO_2 electrode (Fig. 2b), was found to be ~50 F g^{-1} (20 mF cm^{-2}/0.4 mg cm^{-2}), considering that the whole load of RuO_2 takes part in the charging process.

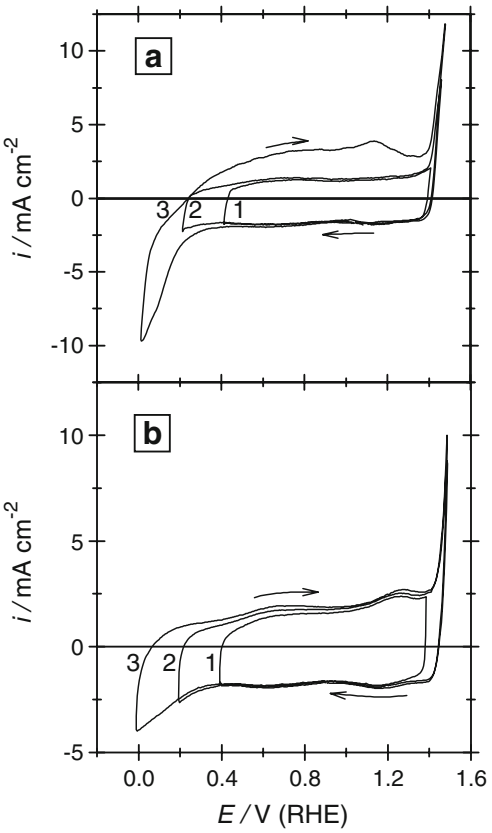

Fig. 1 Cyclic voltammograms of **a** electrochemically and **b** thermally formed RuO_2 electrodes in 0.5 M H_2SO_4, v=50 mV s^{-1}, 293 K

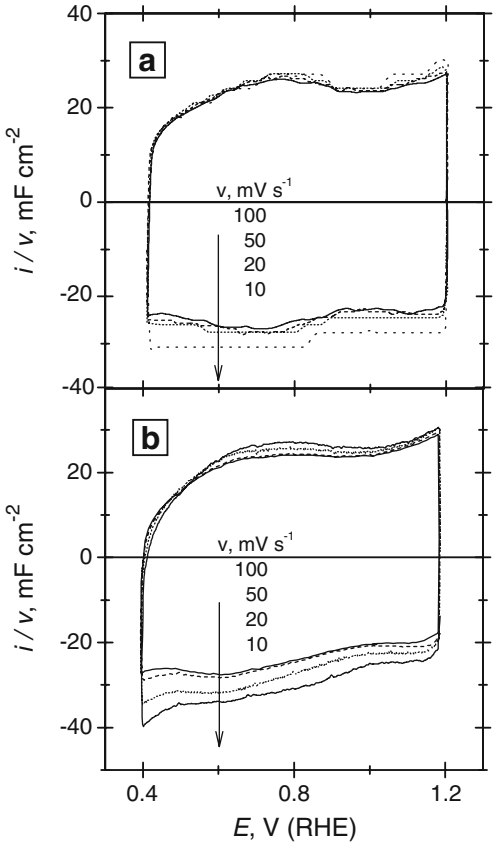

Fig. 2 Capacitance ($C=i/v$) of **a** electrochemically and **b** thermally formed RuO_2 electrodes at various scan rates in 0.5 M H_2SO_4, 293 K

As can be seen from Fig. 2a and b, the average value of capacitance of electrochemically and thermally formed RuO_2 electrodes within the E region of interest ranges between 20 and 25 mF cm^{-2}. Presuming that the electrode behaves like double-layer capacitor and assuming that double layer charge of ideal crystalline RuO_2 surface makes 40–80 μF (real cm^{-2}; [4, 12, 18]), the ratio of true to apparent surface area or the surface roughness factor f of electrochemically and thermally formed RuO_2 electrode would be in the range of roughly 300 to 600, and consequently, the specific area of the electrodes would range between 75 to 150 m^2 g^{-1} (300 or 600/0.4 mg cm^{-2}). This, however, makes just a small portion, about 5%, of the maximum theoretically possible surface area of RuO_2, which can be imagined as the area of whole load of 0.4 mg RuO_2 spread to a monolayer thickness. It follows, therefore, that to enhance the charge storage efficiency of RuO_2, thin RuO_2 layers should be deposited on the substrates with large surface area, which is already being

done in practice by using electrodes with large specific surface area [1, 2].

SEM images of electrochemically formed RuO_2 electrode are presented in Fig. 3. SEM of thermally formed RuO_2 specimen have disclosed typical, cracked-mud-looking surface [19] and are not shown here. Figure 3a reveals the surface covered with spherical particles having size distribution from ~0.5 to ~2 μm and separated in places by cracks of about 0.2 μm width. The surface area of these spheres cannot account for the above-indicated value of surface roughness factor. A closer look into this structure (Fig. 3b) shows that the surface of spherical particles is rugged, i.e., it has its own nano/microstructure. The issue of "inner" and "outer" active surface of RuO_2 electrodes has been widely discussed in Ardizzone et al. [20].

In our recent study [16], it has been suggested that in the case of electrochemically or thermally formed RuO_2 electrodes in 0.5 M H_2SO_4, non-faradaic capacitative current represents the main component of the anodic and cathodic current within E range between 0.6 and 1.2 V. This current has been ascribed to reversible adsorption/desorption of OH^- ions on the surface of RuO_2 phase. It is well known that the structural unit of rutile-type RuO_2 is RuO_6 octahedron [8]. In the basal plane of this octahedron, Ru^{4+} ion is surrounded by four O^{2-} ions. When such plane is situated at the electrode/solution interface, H_2O molecule can occupy the axial position of octahedron above the Ru^{4+} center. In the course of anodic polarization within E range between 0.4 and 1.4 V, H_2O can be replaced by adsorbed OH^- ions, thus forming the $RuO_2^+ \cdot (OH^-)_{ad}$ ionic pair as described by the following equation:

$$RuO_2 \cdot H_2O \Leftrightarrow RuO_2^+ \cdot (OH^-)_{ad} + H^+ + e^-_{(CB)}, \quad (3)$$

where RuO_2^+ and $e^-_{(CB)}$ represent holes and electrons in valence and conduction bands, respectively. This presumption is based on the literature data evidencing the p-type semiconductive nature of RuO_2 oxide [21–24]. According to Chueh et al. [23] and De Almeida and Ahuja [24], there is a small energy gap between oxygen 2*p* and metal *d* bands in RuO_2; thus, the generation of RuO_2^+ holes should be possible under conditions of anodic polarization. The positive charge of RuO_2^+ holes can be compensated by adsorption of OH^- ions, which is the result of dissociation of adsorbed H_2O molecules (Eq. 3). One can see that Eq. 3 is consistent with the stability of RuO_2 phase within the potential range from 0.4 to 1.4 V, as reaction 3 takes place only on the surface of RuO_2 phase and not in the bulk of it as predicted by Eq. 1. On the basis of Eq. 3, it is also easy to understand the above-discussed influence of structural water content on the capacitance of $RuO_2 \cdot xH_2O$ and also the high reversibility of the process taking place on RuO_2 electrodes within 0.4–1.4 V. The latter is due to the fact that the process of interest involves potential-dependent electrostatic adsorption of OH^- ions and not the faradaic charge transfer through the interface. Faradaic oxidation of $(OH^-)_{ad}$ ions with formation of molecular oxygen begins at ~1.4 V [25], as already mentioned. Moreover, it can be shown that charge equivalent to the monolayer of $(OH^-)_{ad}$ ions on ideal RuO_2 surface (i.e., with f=1) is ~0.05 mC cm^{-2}. Considering the fact that the process of interest (Eq. 3) takes place within E range of ~1 V, i.e., from 0.4 to 1.4 V, the resulting capacitance of the RuO_2/electrolyte interface would be ~50 μF cm^{-2}, which falls into the range of C values typical for double-layer charging process, as indicated above [4, 12, 18].

The pseudocapacitance, C_{PC}, manifests itself in the charge storage mechanism of RuO_2 electrodes when the potential range is extended to cover the region where RuO_2 can be partly reduced to metallic ruthenium, which, in turn, can be subsequently oxidized during the anodic scan as in Fig. 1a, cycle 3.

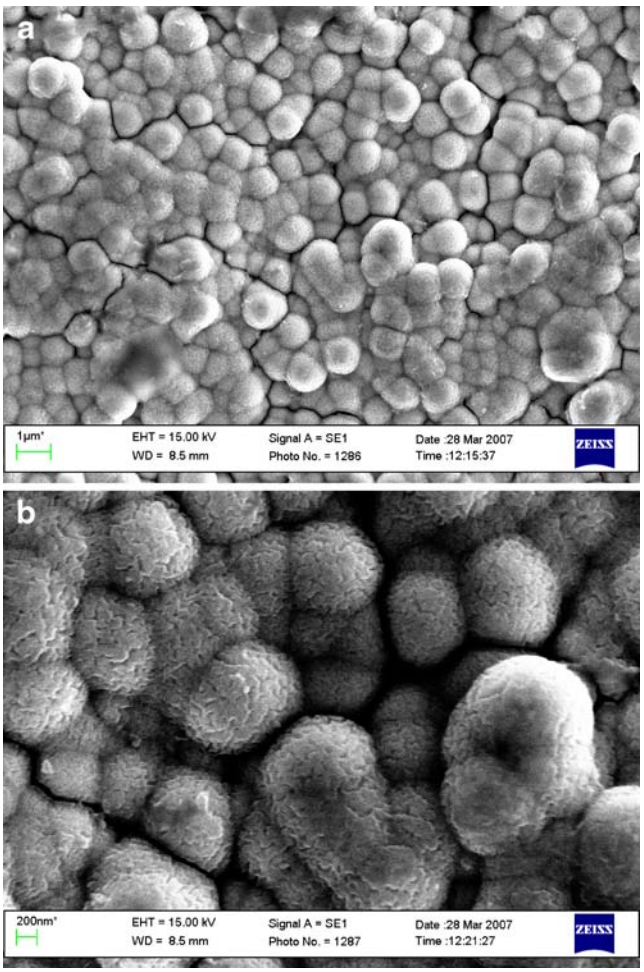

Fig. 3 SEM images of electrochemically formed RuO_2 electrode. **a** General view of surface morphology. **b** Closer view of nano/microstructure of spherical particles

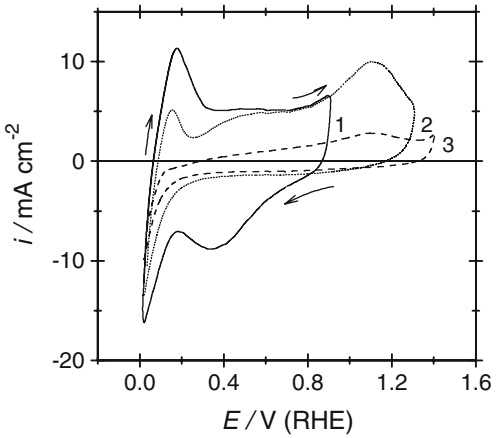

Fig. 4 Cyclic voltammograms of ruthenium coating on Ti substrate in 0.5 M H_2SO_4, v=50 mV s^{-1}, 293 K

Figure 4 shows selected cyclic voltammograms of ruthenium electrode prepared in the form of Ru coating on Ti substrate in 0.5 M H_2SO_4. The curves in Fig. 4 demonstrate clearly the transition from active to passivated state of ruthenium electrode surface. The active state of metallic ruthenium electrode (Fig. 4, cycle 1) is characterized by distinct H_{ad} oxidation peak at ~0.2 V on the positive-going part of the curve [26]. This peak overlaps the first anodic current wave at 0.2 V<E<0.8 V, which represents the process of ruthenium anodic oxidation to $Ru(OH)_3$ possibly through the intermediate stage of $Ru(OH)_2$ formation [16]. Cathodic part of the cycle displays current peak centered at ~0.4 V, reflecting the reduction of $Ru(OH)_3$ to Ru and the beginning of H^+ reduction to H_{ad} at E<0.2 V. Cycle 2 in Fig. 4 encompasses the range of hardly reducible RuO_2 surface oxide formation at 0.8 V<E<1.3 V [14, 27] according to the following overall reaction:

$$Ru + 2H_2O \Leftrightarrow RuO_2 + 4H^+ + 4e^-. \quad (4)$$

With formation of this oxide, passivation of ruthenium surface occurs, what is reflected by the shift of cathodic reduction process to more negative E values compared with cycle 1 and also the suppression of H_{ad} oxidation peak at ~0.2 V. The reduction of the surface oxides in cycle 3 is even more difficult and continues also after the reversal of potential scan at 0 V; no peak attributable to H_{ad} oxidation can be discerned in cycle 3, whereas anodic peak at ~1.1 V becomes significantly suppressed as well. Note that the latter peak corresponds to the anodic wave observed in the voltammogram of RuO_2 electrode in the vicinity of 1.2 V in cycle 3 of Fig. 1a. The comparison of cycle 3 in Fig. 4 and cycle 3 in Fig. 1a shows that the latter one reflects irreversible partial reduction of RuO_2 to metallic ruthenium at E<0.2 V [27] and subsequent oxidation of Ru back to RuO_2 through the stage of $Ru(OH)_3$ formation.

Thus, from the above discussion, it becomes evident that once the surface of ruthenium electrode is passivated with the layer of RuO_2, potential cycling within 0.4–1.4 V produces no further changes, i.e., no faradaic processes occur to a greater extent, and RuO_2/0.5 M H_2SO_4 interface behaves like double-layer capacitor. However, if the potential cycling range is extended to more cathodic potentials, i.e., E< 0.4 V, which is the case often reported in literature [1, 2, 10–13, 18], cathodic reduction of RuO_2 layer sets in. This leads to partial activation of the RuO_2 electrode and subsequent repassivation at E>1.1 V during the anodic process. These faradaic redox processes are mainly responsible for the contribution of pseudocapacitance in the overall capacitance of RuO_2 electrode in 0.5 M H_2SO_4.

The pseudocapacitance, C_{PC}, depends on the nature of electrochemical processes taking place on the electrode surface, whereas the specific pseudocapacitance, C_{PC}^{sp}, is dependent also on the amount of ruthenium compounds, m, taking part in these processes. However, if the contribution of pseudocapacitance in the overall capacitance of $RuO_2{\cdot}xH_2O$ electrodes is limited, and only a certain part of $RuO_2{\cdot}xH_2O$ is electrochemically active, as discussed above, the use of whole mass of $RuO_2{\cdot}xH_2O$ load for the calculation of C_{PC}^{sp} is unjustified. The formula generally used in literature for the evaluation of the theoretic value of $RuO_2{\cdot}xH_2O$ specific pseudocapacitance is as follows:

$$C_{PC}^{sp} = Q/\Delta E\, m = C_{PC}/m = nF/M_{RuOx}\Delta E, \quad (5)$$

where n stands for number of electrons exchanged in the redox process, F is Faraday constant, M_{RuOx} is molecular weight of $RuO_2{\cdot}xH_2O$, and ΔE is the potential window [1, 2, 10]. The ambiguity of such calculations stems also from the uncertainty regarding the redox processes involved in pseudocapacitative charging: n is usually taken to be 2 or 4 [1, 10], presuming the redox process to be transition between Ru(II)/Ru(IV) or Ru(II)/Ru(VI), respectively. Moreover, the values of stoichiometric coefficients x and

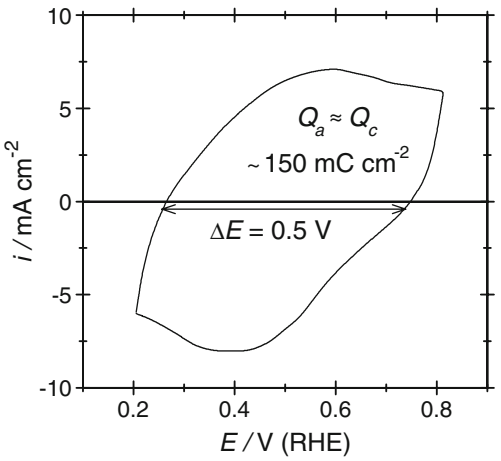

Fig. 5 Cyclic voltammogram of ruthenium coating on Au underlayer in 0.5 M H_2SO_4, v=20 mV s^{-1}, 293 K

n in $RuO_x \cdot nH_2O$ for the calculation of M_{RuOx} are usually taken arbitrarily [1, 2].

Precise evaluation of C_{PC} and C_{PC}^{sp}, eliminating the above flaws, can be done for the faradaic process of ruthenium anodic oxidation to $Ru(OH)_3$ and its reversible reduction as shown in Fig. 5, where the voltammogram of ruthenium electroplated on gold substrate in 0.5 M H_2SO_4 is presented. This particular range of potentials, i.e., from 0.2 to 0.8 V, has been chosen because it corresponds mainly to redox transition $Ru \Leftrightarrow Ru(OH)_3$ as expressed by:

$$Ru + 3H_2O \Leftrightarrow Ru(OH)_3 + 3H^+ + 3e^-. \quad (6)$$

At $E<0.2$ V, reduction of H_3O^+ sets in, whereas at $E>0.8$ V, formation of passivating RuO_2 layer begins as discussed above (see Fig. 4). The passivation of Ru electrode may be also caused by interaction with oxygen from the air, and that is why measurements depicted in Fig. 5 were carried out in inert atmosphere. The presence of Ru^{3+} at 0.4 V and Ru^{4+} at 1.2 V has been confirmed by X-ray absorption measurements in [28]. Analysis of the cycle in Fig. 5 shows that both the anodic or cathodic charge, which makes ~150 mC cm^{-2}, brings the anodic or cathodic shift in Ru electrode potential of about 0.5 V. Consequently, C_{PC}= 150 mC cm^{-2}/0.5 V=300 mF cm^{-2}. In accordance with Eq. 5, the specific pseudocapacitance of this process is $3.8 \cdot 10^3$ F g^{-1}. The latter value is about 75 times higher when compared with $C^{sp} \approx 50$ F g^{-1} obtained for thermally prepared RuO_2 electrode (Fig. 1b). The highest experimentally determined values of the overall specific capacitance C^{sp} of $RuO_2 \cdot xH_2O$ electrodes reported in literature are 1,340 and 1,580 F g^{-1} [1, 2]. They were obtained using nanostructured and microporous electrodes with large specific surface area. These values result from the superposition of faradaic and non-faradaic charging processes in proportions dependent on the experimental conditions and the actual state of the electrode surface.

Conclusions

1. It has been suggested that double-layer-type capacitance of RuO_2/0.5 M H_2SO_4 interface within E range between ~0.4 and ~1.4 V is related mainly to highly reversible non-faradaic process of $RuO_2^+ \cdot (OH^-)_{ad}$ ionic pair formation and annihilation as expressed by summary equation:

   $$RuO_2 \cdot H_2O \Leftrightarrow RuO_2^+ \cdot (OH^-)_{ad} + H^+ + e^-_{(CB)},$$

   where RuO_2^+ and $e^-_{(CB)}$ represent holes and electrons in valence and conduction bands, respectively.
2. In the case when RuO_2 layer is partly reduced at $E<$ 0.2 V, the contribution of pseudocapacitance in the charge storage mechanism of RuO_2 electrodes increases due to faradaic processes related to partial destruction and recovery of the oxide layer.
3. Pseudocapacitance C_{PC} of electrochemically active Ru/0.5 M H_2SO_4 interface within E range between ~0.2 and ~0.8 V is determined by reversible faradaic process as follows:

   $$Ru + 3H_2O \Leftrightarrow Ru(OH)_3 + 3H^+ + 3e^-$$

   with theoretic specific pseudocapacitance value $C_{PC}^{sp} = 3.8 \cdot 10^3 F\ g^{-1}$.

References

1. Hu CC, Chen WC, Chang KH (2004) J Electrochem Soc 151 A:281
2. Hu CC, Chen WC (2004) Electrohim Acta 49:3469
3. Conway BE (1991) J. Electrochem Soc 138:1539
4. Conway BE (1999) Electrochemical supercapacitors. Plenum, New York
5. Liu T, Pell WG, Conway BE (1997) Electrochim Acta 42:3541
6. Trasatti S, Buzzanca G (1971) J Electroanal Chem 29:App. 1
7. Trasatti S (1980) Electrodes of Conductive Metallic Oxides, Parts A, B. Elsevier, Amsterdam
8. McKeown DA, Hagans PL, Carette LP, Russell AE, Swider KE, Rolison DR (1999) J Phys Chem B 103:4825
9. Ma Z, Zheng JP, Fu R (2000) Chem Phys Lett 331:64
10. Zheng JP, Cygan PJ, Jow TR (1995) J Electrochem Soc 142:2699
11. Ahn YR, Song MY, Jo SM, Park CR, Kim DY (2006) Nanotechnology 17:2865
12. Sugimoto W, Kizaki T, Yokoshima K, Murakami Y, Takasu Y (2004) Electrochim Acta 49:313
13. Sugimoto W, Yokoshima K, Murakami Y, Takasu Y (2006) Electrochim Acta 52:1742
14. Burke LD, Naser NS (2005) J Appl Electrochem 35:931
15. Juodkazytė J, Šebeka B, Valsiūnas I, Juodkazis K (2005) Electroanal 17:947
16. Juodkazytė J, Vilkauskaitė R, Stalnionis G, Šebeka B, Juodkazis K (2007) Electroanal 19:1093
17. Santos MC, Terezo AJ, Fernandes VC, Pereira EC, Bulhoes LOS (2005) J Solid State Electrochem 9:91
18. Doubova LM, Daolio S, De Battisti A (2002) J Electroanal Chem 532:25
19. Terezo AJ, Pereira EC (2002) Mat Lett 53:339
20. Ardizzone S, Fregonara G, Trasatti S (1990) Electrochim Acta 35:263
21. Patil PS, Ennaoui A, Lokhande CD, Muller M, Giersig M, Diesner K, Tributsch H (1997) Thin Solid Films 310:57
22. Gujar TP, Shinde VR, Lokhande DC, Kim WY, Jung KD, Joo OS (2007) Electrochem Comm 9:504
23. Chueh YL, Hsieh, Chang MT, Chou LJ, Lao, Song JH, Gan JY, Wang ZL (2007) Adv Mater 19:143
24. De Almeida JS, Ahuja R (2006) Phys Rev B 73:165102
25. Juodkazytė J, Vilkauskaitė R, Šebeka B, Juodkazis K (2007) Trans Met Finish 85:194
26. Michell D, Rand DAJ, Woods R (1978) J Electroanal Chem 89:11
27. Pourbaix M (1963) Atlas d'equilibres electrochimiques. Gauthier-Villars, Paris
28. Mo Y, Antonio MR, Scherson DA (2000) J Phys Chem B 104:9777